Semiconductor Optoelectronics
ISSN: 1001-5868

# INFLUENCE OF SAMARIUM ION SUBSTITUTION ON STRUCTURAL, ELECTRICAL, AND MAGNETIC PROPERTIES OF CO-MG NANO-FERRITES

**Banothu Naresh[1] , J.Laxman Naik[1,*]**
[1]Department Of Physics, University College of Science, Osmania University Hyderabad, Telangana 500007, India.
*Corresponding Author: laxmannaikj@gmail.com

**Abstract:**

$Co_{0.2}Mg_{0.8}Sm_xFe_{2-x}O_4$ ($x = 0.00 \leq x \leq 0.025$) has been prepared using the Sol gel combustion method from powders Of Co, Mg, Fe, and Sm nitrates, which were used as starting materials. To better understand the structure morphology properties, XRD, FESEM, HRTEM, FTIR, Ac and Dc conductivity and magnetic property analyses were done. An x-ray diffraction (XRD) investigation confirmed the creation of a spherical structure with a crystal size of between 33 and 39 nm. It was revealed that the increased doping concentration of Samarium ($Sm^{3+}$) increases the lattice parameters of the crystal. The X-ray density increases as the concentration of $Sm^{3+}$doping increased. X-ray density increases due to the $Sm^{3+}$ion's larger molar mass than the $Fe^{3+}$ion. Analysis by FESEM indicated that the particles have an irregular size and a high concentration of open pores. It was discovered that ferrite nanoparticles have a spherical in structure with an average size of 75nm can be seen clearly by TEM. According to the FTIR spectra, the primary absorption bands associated with the tetrahedral and octahedral metal-oxygen bonds are located in the region of (350-4000$cm^{-1}$). Dielectric spectroscopy revealed Maxwell-Wagner interfacial polarisation, which diminishes with increasing applied field frequency. The sample has a dielectric loss of less than 8, indicating it may be used to fabricate multilayer inductors. The decreases in g-value are well correlated with the variation of particle size. The hopping model explained why the ac conductivity of the samples rose with increasing doping and frequency. Samples with samarium contents of 0.015 and 0.000 showed high impedance stability at room temperature , rendering them suitable for use as a high-frequency. A rise in $Sm^{3+}$ concentration increased M-H loop saturation magnetization (Ms), coercivity (Hc), and retentivity (Mr). The values of Ms and Hc varied anisotropically with Sm doping. The findings of this study suggest that zinc cobalt ferrite doped with samarium might be beneficial for magnetic resonance imaging in biomedicine.

**Keywords:** Samarium, ferrite, nanoparticle; XRD, FESEM, HRTEM, FTIR, Electrical and magnetic properties

## 1. INTRODUCTION

Even many years after their development, ferrite materials still have great curiosity in the scientific community as well as commercial applications due to their remarkable properties in both nano and bulk form. Scientists, researchers, technologists, and engineers have put in a significant amount of work to discover new commercial uses for ferrites with extraordinary features [1, 2]. Because of its outstanding electrical resistivity, mechanical hardness, chemical

stability, and low cost, Co-Mg has piqued the curiosity of many researchers [3]. As a result of its exceptional characteristics, Co-Mg is an excellent candidate for use in a variety of applications, including microwave devices, memory devices, and transformer centers [4]. The mixed spinel structure $(Mg^{2+}Fe^{2+})$ $[Co^{2+}Fe^{3+}]$ $O_4^{-2}$ was observed in Co-Mg ferrite [1], in which $Mg^{2+}$ and $Fe^{2+}$ occupy A site while $Co^{2+}$ and $Fe^{3+}$ occupy B site, has been discovered in this material. In addition to the technique and circumstances of preparation, as well as the quantity and kind of additives used, the characteristics of ferrites are impacted by many other factors. Due to their higher ionic radius, rare-earth implantation can fine-tune the structural, electrical, and magnetic properties of ferrites [5–11]. In ferrites, changing the cation dispersion between the A and B sites for divalent ($M^{2+}$) or ferric ($Fe^{3+}$) ions changes the cation dispersion. The structural, electrical, and soft magnetic properties of Co-Mg ferrites have been altered by the addition of substituted Ni, Si, and Mo atoms. [11-13]. Electron hopping between $Fe^{2+}$ and $Fe^{3+}$ is the main contributor to the electrical conductivity of spinel ferrites (generated through the sintering procedure [14, 15]) and $Fe^{3+}$ ions at the octahedral (B) site [16]. The octahedral (B) site is occupied by rare-earth ions, which limits electron hopping by restricting the mobility of $Fe^{+2}$ and increasing resistivity [8–10]. Some rare-earth ions, such as $Gd^{3+}$ and $Ho^{3+}$, have previously been successfully replaced in the CoZn ferrites [9.10]. By substituting $Sm^{3+}$ for $Fe^{3+}$ in $Co_{0.2}Mg_{0.8}Sm_xFe_{2-x}O_4$ ($x = 0.00 \leq \chi \leq 0.0025$ in a step of 0.005), the electrical resistivity of Co-Mg ferrites to compositions of $Co_{0.2}Mg_{0.8}Sm_xFe_{2-x}O_4$ ($x = 0.00 \leq \chi \leq 0.0025$ in a step of 0.005) has been expected to be increased, and it was expected that a significant characteristic (rise resistivity) would be obtained. Furthermore, in the ferrites Ni-Zn, Mg, Mg-Zn, and Co, the element samarium (Sm) was previously substituted [17–25]. To our knowledge, no research has been done on the effects of Sm replacement in Co-Mg ferrite. As a result, we present here the replacement of the $Sm^{3+}$ ion for $Fe^{3+}$ in Co-Mg ferrites with compositions of $Co_{0.2}Mg_{0.8}Sm_xFe_{2-x}O_4$ (where $x = 0.00 \leq \chi \leq 0.025$), which provides useful information for practical applications [26].

## 2. MATERIALS AND METHOD

### Materials

The Sm-doped Co–Mg ferrite nanoparticles were made with analytical grade (AR) ingredients that did not require further purification. The ferrites were made using cobalt nitrate hexahydrate ($Co(NO_3)_2 \cdot 6H_2O$), magnesium nitrate hexahydrate ($Mg(NO_3)_2 \cdot 6H_2O$), ferric nitrate hexahydrate ($Fe(NO_3)_3 \cdot 9H_2O$), and samarium nitrate hexahydrate ($Sm(NO_3)_3 \cdot 6H_2O$). The production of the Co–Mg ferrite nanoparticles was carried out using triple-distilled water.

### Method

The samarium ion substitution these Co–Mg ferrite powders ($Co_{0.2}Mg_{0.8}Sm_xFe_{2-x}O_4$) with a m/o of (x = 0.000, 0.005, 0.010, 0.015, 0.020, 0.025) were made using the citric sol–gel auto-combustion process. Citric acid was employed 1:3 with metal nitrate as a cation-exchange chemical. The stoichiometric weights of ($Co(NO_3)_2 \cdot 6H_2O$), ($Sm(NO_3)_2 \cdot 6H_2O$),and ($Mg(NO_3)_2 \cdot 6H_2O$), were used to start the hydrolysis process $(NO_3)_3 \cdot 6H_2O$), ($C_6H_8O_7 \cdot H_2O$), and ($Fe(NO_3)_3 \cdot 9H_2O$), were all dissolved in distilled water and heated for 1 hour at 250°C with constant stirring. To keep the $PH^7$, added the ammonia solution drop by drop. Using an electrically controlled magnetic stirrer and heater, the solution is allowed to heated to 150°C on a hot plate for 15 to 20 minutes. The solution is continuously stirred and heated, resulting in an extremely thick, viscous, dark-colored gel. Continue to heat the gel until all water

molecules have been removed, resulting in the start of the gel's combustion. Shortly after auto-ignition, the gel burns down to soft ash. The powder was grounded with an agate mortar for up to 3 hrs. In a temperature controlled furnace, the powder was annealed at 700°C up to 5 hours, until it was hard. The KBr pellet method was used to prepare pellets in the shape of discs with diameters of 15 mm and a thickness of 2 mm from ferrite powders. Silver paste was used on both sides of the pellets to achieve good ohm connections. These pellets were used in electrical and dielectric investigations.

**Characterization**

X-ray diffraction (XRD; Rigaku Miniflex-600, Japan) was used to characterise nanoparticles utilising CuK radiation (= 1.5405) from 20° to 80° and a scanning rate of 2 min. The surface morphology was examined using a FESEM, (FESEM; Oxford Instrument Inca X-act) and energy-dispersive X-ray (EDX) examination at a 200 kV accelerating voltage. A HRTEM was used to examine the cross-sections and particle sizes of the nanoparticles (HRTEM, JEM-F200 Multi-purpose Electron Microscope). The KBr pellet technique was used to measure Fourier-transform infrared (FTIR) spectroscopy using an IR spectrometer (FTIR-8400S Shimadzu). By tracing M-H curvatures, saturation magnetization, remanance, and coercive field for the powder sample were determined at room temperature using the vibrating sample magnetometer (VSM) model Lake Shore Cryotronics 8600 Series. The dielectric tests were completed with the help of the (Novocontrol GmBH, Alpha-A High Performance Frequency).

## 3. RESULTS AND DISCUSSION

### 3.1. XRD Analysis

The X-ray diffraction pattern is the same for all $Co_{0.2}Mg_{0.8}Sm_xFe_{2-x}O_4$ ($0.000 \leq \chi \leq 0.025$) spinel ferrite nano particles made by the sol-gel auto combustion method. Sintered for 5 hours at 700°C, Co-Mg composite samples were created. The XRD method was used to determine the crystal structure and crystalline phase pattern of the substance. This is a highly useful approach for estimating the parameters of crystalline structures. XRD analysis revealed the most intense peak at $2\theta = 35$ for a cubic spinel structure. Identical to the peak of Co-Mg ferrite, all of the peaks with hkl are (111), (220), (311), (222), (400), (422), (511), (440), (440), and (533). The positions and miller indices of the peaks suggest that an FCC type spinel structure has formed. All of the peaks in the pattern are well defined and matches with the JCPDS file no 22-1086, indicating that the ferrites used in the preparation have an FCC spinel structure too [27. 28].

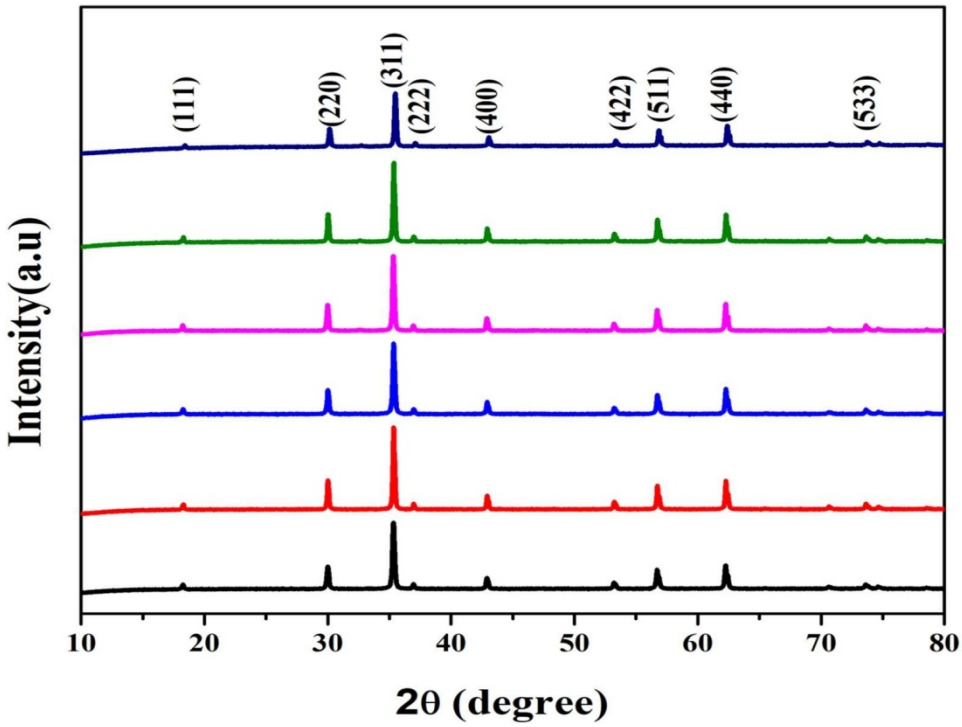


Fig.1. X-ray Diffraction pattern of $Co_{0.2}Mg_{0.8}Sm_xFe_{2-X}O_4$ nano-ferrites ($x$= 0.000, 0.005, 0.010, 0.015, 0.020, and 0.025).

Figure 1 shows the XRD patterns of the doped Co-Mg composition, and it is found that no impurity peaks were found. The XRD Debye Scherrer formula was used to compute the crystallite size ($D_m$) [28]:

$$D_m = \frac{k\lambda}{\beta\cos\theta}\ (nm) \qquad (1)$$

Where 'K' =0.9 for spinel ferrites, 'λ' = 1.5406 A° is the x-ray beam wavelength and 'β' is the FWHM of the most intense peak and 'θ' is the angle of the most intense peak. The crystallites size was estimated to be between 21.32 and 26.74 nm, which are absolutely small. Because of the increasing concentration of $Sm^{3+}$ doping, the size of the crystallites rises, and they are now in this same range of 21.32 nm (0.000) to 26.74 nm (0.025) [29, 30]. The formula for calculating the average lattice constant is as follows:

$$a = d\sqrt{h^2 + k^2 + l^2}\ \text{Å} \qquad (2)$$

The crystal plane spacing is 'd', and the miller index values are hkl. For all the samples, the average lattice constant ranges from 8.03A° to 8.89A°. The average lattice constant 'a' was computed using $Sm^{3+}$ and $Fe^{3+}$ ionic radii. It was observed that when the m/o of $Sm^{3+}$ doping was increased, the average lattice constant increased as shown in Fig 1 [31].

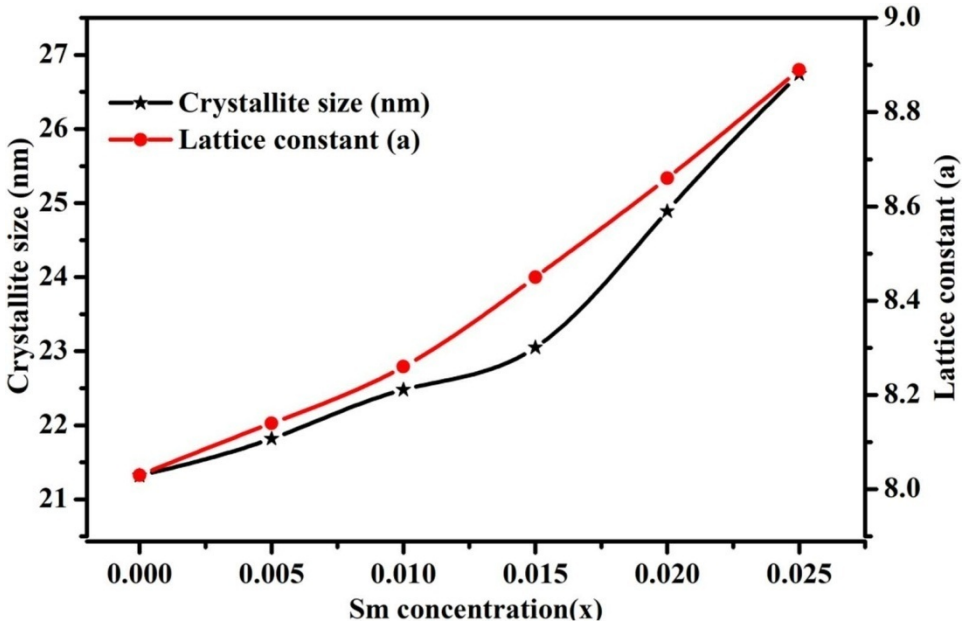


**Fig.2.**The variation of the Lattice constant and Crystallite size for $Co_{0.2}Mg_{0.8}Sm_xFe_{2-x}O_4$ nano-ferrites ( x= 0.000, 0.005, 0.010, 0.015, 0.020, and 0.025)

The formula for calculating the X-ray density $\rho_x$ as follows:

$$\rho_x = \frac{8M}{Na3} \ (g/cm^3) \qquad (3)$$

Where 'M' is the composition's molecular weight, 'Z' = 8 is the number of molecules per unit cell, 'N' is indeed the Avogadro number ($6.0238x10^{23}$), and for '$a^3$' is the volume of a unit cell. The density of X-rays was determined to be between 5.60 g/cm$^3$ to 5.99 g/cm$^3$. The relationship between the density of X-rays and their concentration $Sm^{3+}$. As the quantity of $Sm^{3+}$ doping rises, the X-ray density initially increases, then drops. These differences are due to the greater molecular weight of $Sm^{3+}$ [32]. The bulk density of the pellets may be calculated using the relation:

$$\rho_m = \frac{m}{v} \qquad (4)$$

The pellets' mass is 'm' and their volume is 'v'. On average, 3.43 g/cm$^3$ to 3.85 g/cm$^3$ were computed. The concentration of $Sm^{3+}$doping causes the bulk density to shows random change and a maximum of 0.025 m/o. As a result, lowering the bulk density lowers the overall weight of pall*e*ts [33].

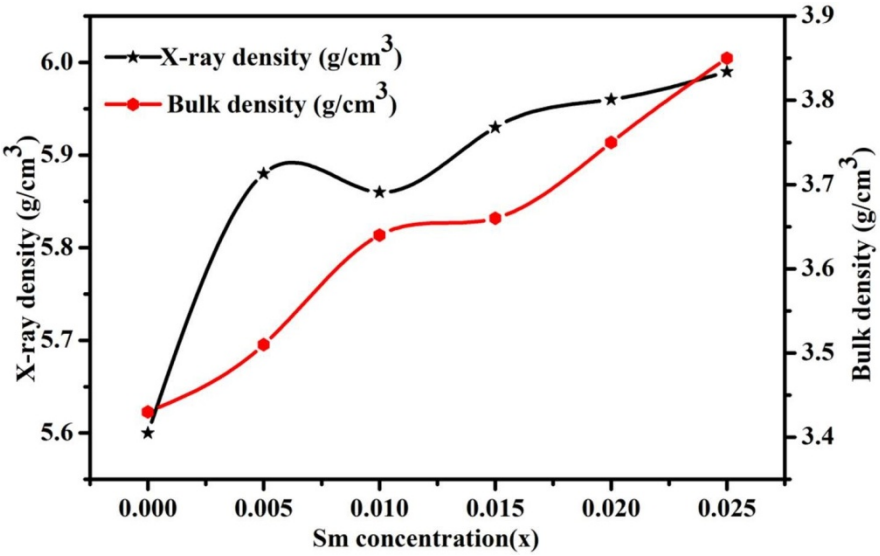


Fig.3.The Variation in the Bulk density and X-ray density of $Co_{0.2}Mg_{0.8}Sm_xFe_{2-x}O_4$ nano-ferrites ( x= 0.000, 0.005, 0.010, 0.015, 0.020, and 0.025)

**Table 1**.Particle size ($D_{Xrd}$), Lattice parameter(a), Volume of unit cell(V), Strain($\varepsilon_s$), jump length of A-site($L_A$) jump length of B-site($L_B$), $Co_{0.2}Zn_{0.8}Sm_xFe_{2-X}O_4$ nano-ferrites ( x=0.000, 0.005, 0.010, 0.015, 0.020, and 0.025).

| Composition($x$) | $D_{Xrd}$(nm) | a(Å) | V(Å$^3$) | $L_A$(Å) | $L_B$(Å) | Strain($10^3$) | Dislocation density |
|---|---|---|---|---|---|---|---|
| 0.000 | 21.32 | 8.03 | 598.14 | 3.54 | 2.79 | 25.20 | 9.823 |
| 0.005 | 21.82 | 8.14 | 598.26 | 3.66 | 2.91 | 22.61 | 8.481 |
| 0.010 | 22.48 | 8.26 | 598.31 | 3.36 | 2.69 | 20.10 | 7.298 |
| 0.015 | 23.05 | 8.45 | 598.49 | 3.86 | 2.79 | 18.24 | 6.250 |
| 0.020 | 24.89 | 8.86 | 598.62 | 3.26 | 2 .59 | 17.18 | 6.433 |
| 0.025 | 26.74 | 8.89 | 598.81 | 3.816 | 2.88 | 14.20 | 5.340 |

**Table 2**. Bulk density($\rho_B$), X-ray density($\rho_x$), porosity(P), Absorption band wave number($V_1$ and $V_2$)From FTIR is spectra, for nanosized $Co_{0.2}Mg_{0.8}Sm_xFe_{2-X}O_4$ nano-ferrites ( x= 0.000, 0.005, 0.010, 0.015, 0.020, and 0.025).

| Composition($x$) | $\rho_x$ (g/cm$^3$) | $\rho_B$ (g/cm$^3$) | P (%) | $V_1$ (cm$^{-1}$) | $V_2$ (cm$^{-1}$) |
|---|---|---|---|---|---|
| 0.000 | 5.60 | 3.43 | 14.001 | 556 | 410 |
| 0.005 | 5.88 | 3.83 | 9.134 | 548 | 401 |
| 0.010 | 5.86 | 3.54 | 9.512 | 553 | 395 |
| 0.015 | 5.93 | 3.66 | 8.587 | 559 | 409 |
| 0.020 | 5.96 | 3.75 | 8.901 | 552 | 403 |
| 0.025 | 5.99 | 3.85 | 7.583 | 555 | 427 |

Using $d_x$ and $d_B$ values, porosity (P) values were calculated and found to be in the range between 14 to 7 percent as the doping m/o is increased (Table 2), indicating that the synthesised materials are porous [34-36].

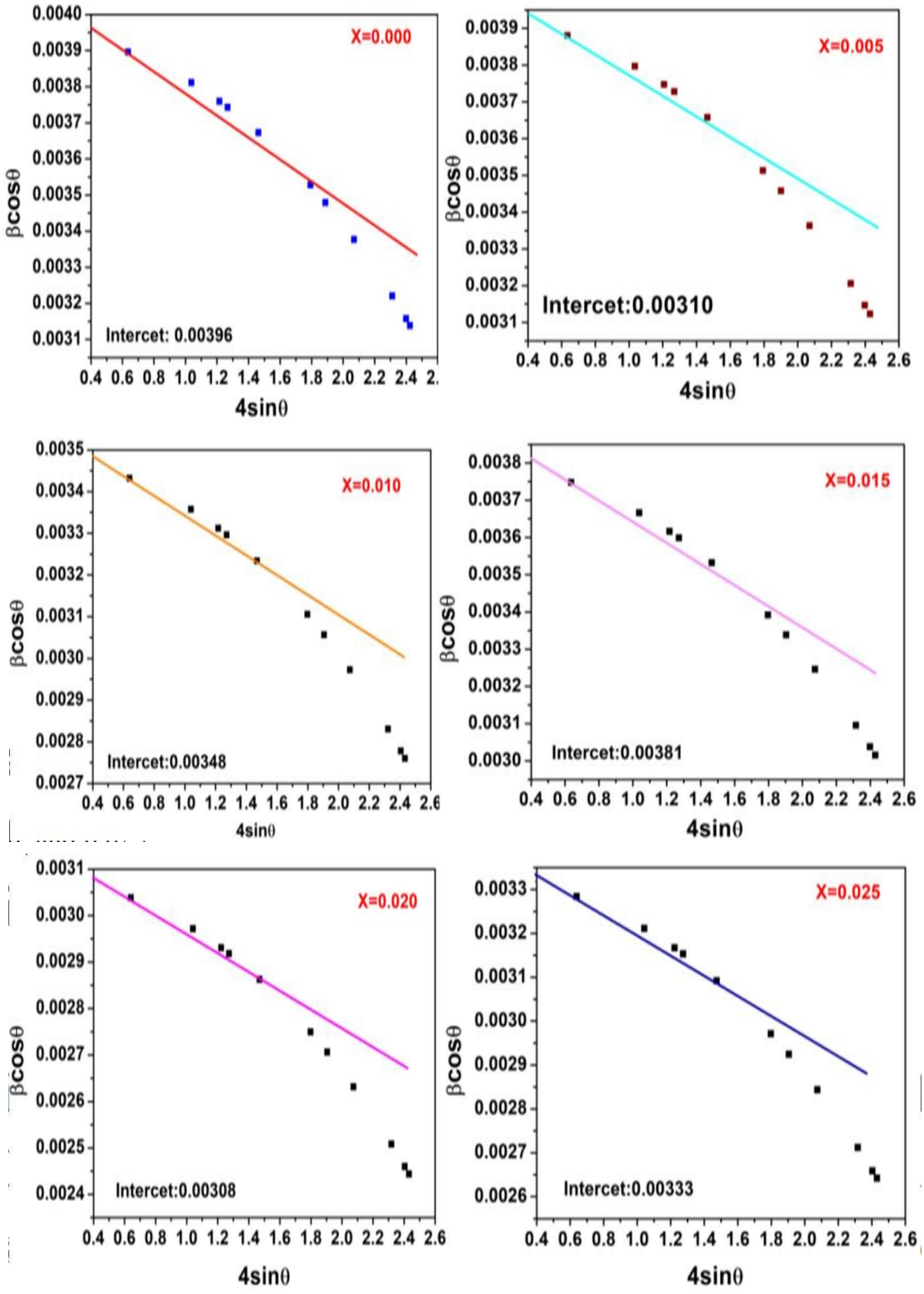

**Fig.4**.Williamson-Hall plot of $Co_{0.2}Mg_{0.8}Sm_xFe_{2-x}O_4$ nano-ferrites x = 0.000, 0.005, 0.010, 0.015, 0.020, and 0.025.

The following formula is used to compute the strain:

$$\varepsilon = \frac{\beta}{4tan\theta}(10^{-3}) \qquad (5)$$

Where '$\beta$' 'is the diffraction angle of the most intense peak. The predicted strain was $14.01x10^{-3}$ to $7.58x10^{-3}$ psi. As the quantity of $Sm^{3+}$ doping is increased, the strain reduces randomly. At a value of x= 0.000, the highest amount of strain was found [37]. To calculate the dislocation density of the nanoparticles produced.

$$\delta = \frac{1}{D2} \qquad (6)$$

Where 'D' is the crystalline size. With increasing m/o of $Sm^{3+}$concentration, the dislocation density decreases at minimum for x=0.000 to 0.025 is 9.82 to 5.34 line/m. The jump length $L_A$ and $L_B$ between both the ions at A and B-site were calculated using the relationship.

$$L_A = \frac{a\sqrt{3}}{4} \qquad (7)$$

$$L_B = \frac{a\sqrt{2}}{4} \qquad (8)$$

In Co-Mg ferrite, the values of jump length $L_A$ are increasing and $L_B$ are decreased with $Sm^{3+}$ increasing composition. This is owing to the fact that the lattice constant lowers with the addition of $Sm^{3+}$ composition [38-40].

## 4. FIELD EMISSION SCANNING ELECTRON MICROSCOPE (FESEM)

Figure 5 depicts the surface morphology or structural investigation of ferrite samples at room temperature using a FESEM for ruptured surfaces. Sm doped $Co_{0.2}Mg_{0.8}Sm_xFe_{2-x}O_4$ ferrites FESEM are shown in Fig 5. According to the high magnification picture at 200 nm, this shows agglomerated nanoparticle morphology, which is composed of secondary irregularly shaped spherical nanoparticles. These nanoparticles are 70 nm–120 nm in size [41]. The presence of Sm-doping in $Co_{0.2}Mg_{0.8}Sm_xFe_{2-x}O_4$ ($0.000 \leq \chi \leq 0.025$) results in increased agglomeration of the spherically nanoparticles, which was accompanied by an increase in the crystalline size [42]. Higher concentrations of Sm agglomerate owing to ferromagnetic $Co^{2+}$ and diamagnetic $Mg^{2+}$ replacement. The magnetic character of the materials is to blame for the agglomeration, which was further verified by VSM analysis [43].

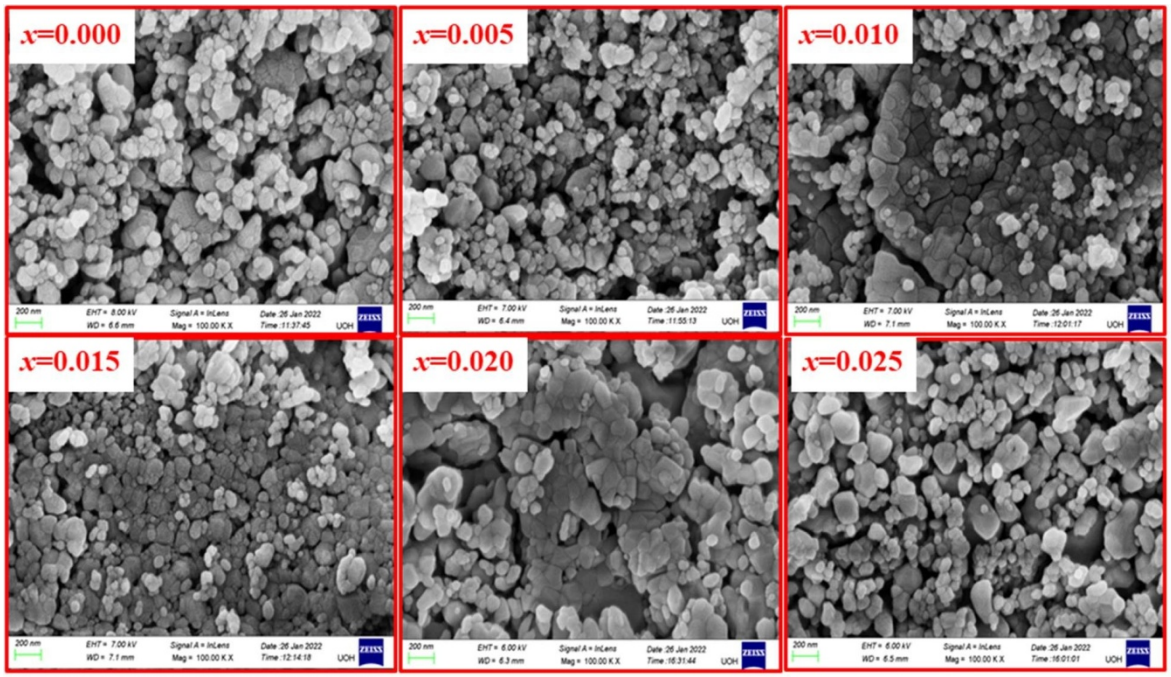


Fig. 5. FE-SEM Images of the $Co_{0.2}Mg_{0.8}Sm_xFe_{2-X}O_4$ nano-ferrites ( x= 0.000, 0.005, 0.010, 0.015, 0.020, and 0.025).

## 5. HIGH-RESOLUTION TRANSMISSION ELECTRON MICROSCOPY (HRTEM)

TEM pictures of the $Co_{0.2}Mg_{0.8}Sm_xFe_{2-X}O_4$ sample are shown in Fig 6. The majorities of nanoparticles have a spherical shape and are seen agglomerated. It is possible that single-phase crystals were formed, as shown by the presence of strong diffraction rings in TEM micrographs [44]. ImageJ software calculated the average particle size to be 74nm. Figure 6 shows the (SAED) pattern of the nanoferrite CMSFO ($x$ =0.000, 0.015, 0.025), which displays patchy diffraction rings that exactly match the diffraction peak obtained from the XRD pattern (see Fig.7), confirming the cubic spinel phase development in $Sm^{3+}$doped Co-Mg nanoferrites. Fig. 6 shows the HRTEM of the nanoferrite ($x$ =0.000, 0.015, 0.025). Several lattice fringes can be noticed. Fringe widths of 0.245, 0.264, and 0.269 nm correspond to the (311) peak, demonstrating that HRTEM and XRD investigation of Co-Mg-Sm nanoferrites are identical.

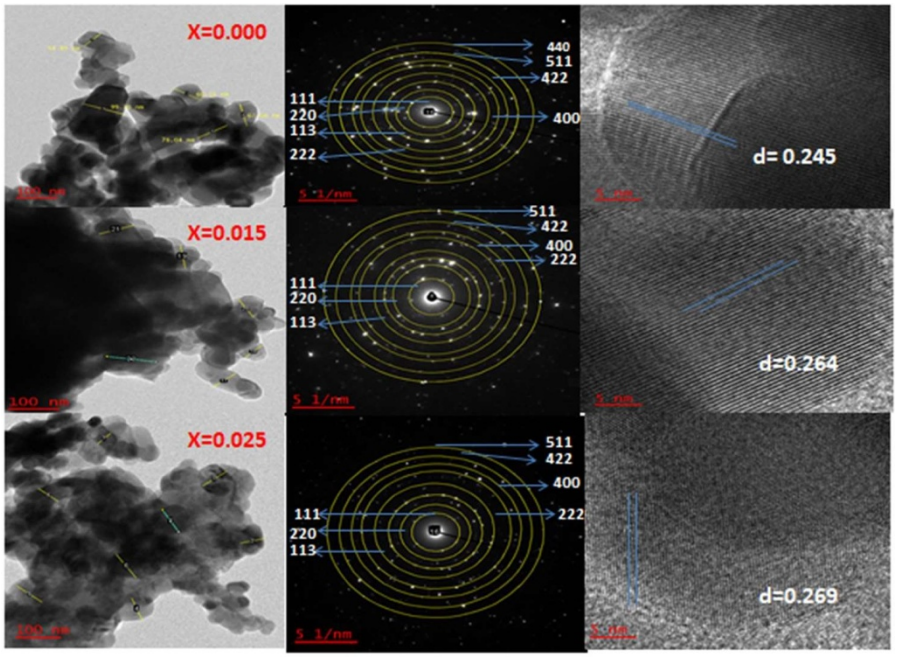


Fig. 6. Show the TEM Micrographs of $Co_{0.2}Mg_{0.8}Sm_xFe_{2-x}O_4$;(where $0.000 \leq x \leq 0.025$, $step\ 0.005$) SAED and HRTEM of nanoferrite with x=0.000,0.015,0.025

## 6. FOURIER TRANSMISSION INFRARED SPECTROSCOPY (FTIR)

The FTIR spectra of nanosized $Co_{0.2}Mg_{0.8}Sm_xFe_{2-x}O_4$ in the 350-4000cm$^{-1}$ range were acquired at room temperature and are shown in Figure 7. The FTIR spectra of all materials exhibit two primary absorption bands in the 350-700 cm$^{-1}$ region. The inherent stretching vibrations of the metal at the tetrahedral $M_{tet}$-O and octahedral $M_{oct}$-O sites are related to these two vibration bands. Tetrahedral complexes are represented by the band that appears at the higher wave number ($v_1$, 548–560 cm$^{-1}$), whereas octahedral complexes are represented by the band that appears at the lower wave number ($v_2$, 395–430 cm$^{-1}$)[45]. By adding $Sm^{3+}$ content, it is possible to determine that the difference in the $Fe^{3+}$ -$O^2$ distance for the octahedral and tetrahedral sites is what causes the difference between the $v_1$ and $v_2$ band locations [46]. In $Co_{0.2}Mg_{0.8}Sm_xFe_{2-x}O_4$ doped with the rare earth element, the $v_2$ band broadens, indicating the occupancy of rare earth ions on the B-sites[47]. Stretching vibrations of the C=O are shown by the peaks between 1630 and 1660 cm$^{-1}$. A stretched hydroxyl (O-H) group that corresponds to a bandwidth between 3435 and 3480 cm$^{-1}$ is seen, signifying the presence of moisture and water. The observed peak between 2330 and 2370 cm$^{-1}$ is caused by the stretching of the C-H bond [48].

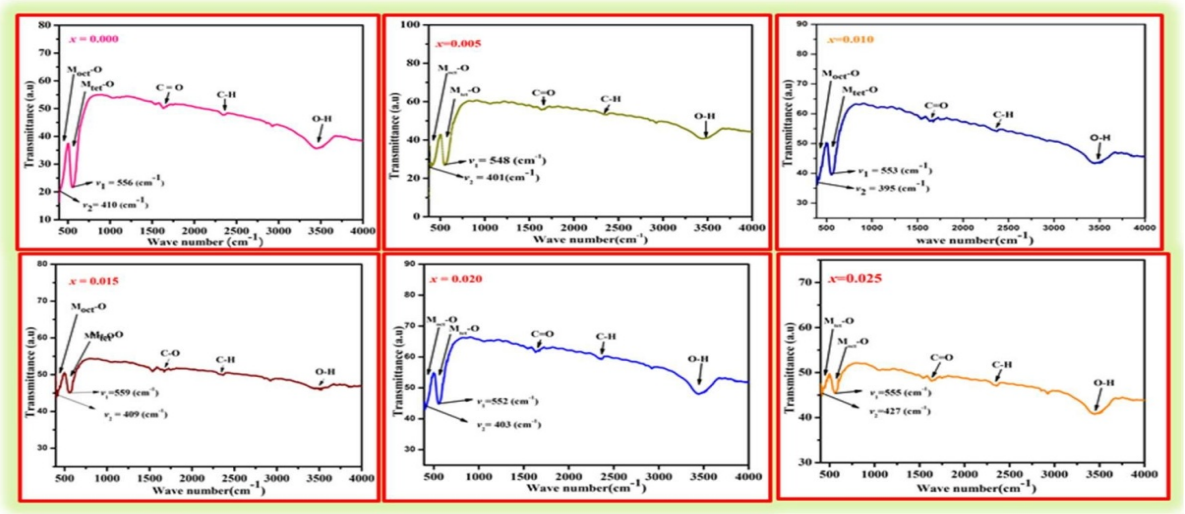


**Fig.7**. FTIR spectra of nanosized $Co_{0.2}Mg_{0.8}Sm_xFe_{2-x}O_4$ nano-ferrites ( x= 0.000, 0.005, 0.010, 0.015, 0.020, and 0.025).

## 7. ELECTRICAL PROPERTIES

### 7.1 Dielectric Measurement

The dielectric dispersion of the samples was examined from 3Hz to 20MHz at room temperature. As shown in Figure 8, a frequency applied field produces Sm-doped Co-Mg ferrite nanoparticles. Interfacial polarisation response of dielectric dispersion decreased with applied field frequency [49-52]. It decreased rapidly up to 7 KHz and reaches to saturation. Because the domains in a dielectric material were initially random, adding a field oriented them in the field's direction.

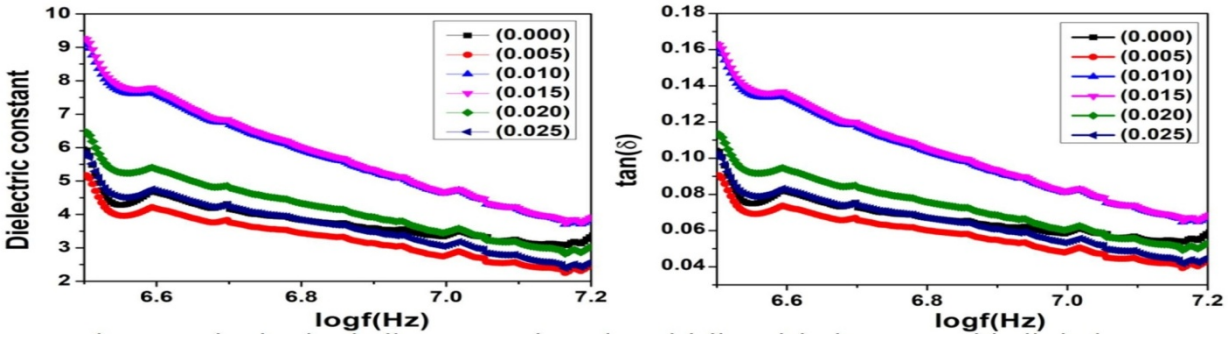


**Fig.8**.dielectric constant spectra of $Co_{0.2}Mg_{0.8}Sm_xFe_{2-X}O_4$ nano-ferrites ( x= 0.000, 0.005, 0.010, 0.015, 0.020, and 0.025).

Initially, the domains aligned with the applied field and responded well to switching. In the study, the domains lagged behind the applied field by over 7MHz. Increasing the amount of Sm doping also increased the dielectric constant, proving that the hopping of charges between charge carriers, originally between $Fe^{3+}$ and $Fe^{2+}$, was successful [53].

Fig 8 represent the frequency dependent dielectric constant for CMSFO systems in the range of 3Hz to20Hz from 700oC. It is observed that dielectric constant is high at lower frequencies and decreases exponentially reaching to constant value at very high frequencies for all Sm doped systems. This is due to the presence of space charge polarization along with other polarizations such as dipolar, ionic and electric. Larger value of dielectric constant for doped system can also be due to the increased number of lattice defects compared to that of pure system. The increase in dielectric with m/o is due to interfacial polarization, grain boundary defect.

### 7.2 Dielectric loss (tan$\delta$)

Dielectric loss is a critical metric in determining a material's viability for electrical applications, notably in capacitors and bridge circuits. Any electronic application requires a dielectric loss of less than unity, suggesting suitability for high resistance applications and ease of manufacture [54]. Figure 10 shows dielectric loss in Co–Mg nanoparticles with Sm doping from 3Hz to 20 MHz. The dielectric loss had a typical response to the applied field frequency, with the loss reducing as the frequency was increased. The dielectric loss is maximum for 0.164

The variation of dielectric loss (tan) with frequency at various temperatures of CMSFO system is shown in Fig 8. It can be noticed that the dielectric loss is maximum at the lower frequencies and found to decrease gradually with frequency. The dielectric loss represents the energy loss that occurs when the polarization lags behind the applied electric field due to the presence of grain boundaries [55]. The loss in these systems could be attributed to various conductions processes. The decrease in dielectric loss with frequency can be explained on the basis of Koops theory. It can also be noticed from Fig that change in dielectric loss with m/o sm and was observed maximum for x=0.015 system [56].

**7.3 AC Conductivity:**

The frequency dependent AC conductivity for different systems was studied at 700C shown in Fig 9. Study of AC conductivity give the electrical transport properties of a material by using jonschers power low [57];

$$\sigma_{AC}(\omega)=\boldsymbol{\sigma}_{DC}+A\omega^{n} \quad (9)$$

Where $\boldsymbol{\sigma}_{DC}$ is frequency independent conductivity at low frequencies. Random diffusion of the charge via activated hopping gives rise to a frequency independent conductivity. At higher frequencies, $\sigma_{AC}$ exhibits increases in dispersion and eventually becoming almost linear. A is the temperature dependent pre-exponential factor and n is the frequency independent exponent, but depends on temperature and material. The increasing value of $\sigma_{AC}$ with frequency is due to the hopping of cations between the neighboring of sites. Also, increases of conductivity with temperature could be due to the thermally activated processes. From the Fig 9 the enhancement of conductivity was observed maximum for 9.027 m/o, high could be due to presence of large number of charge carriers and the increases rate of hopping, there after a decreases in the conductivity was noticed for further increases in Sm concentration which could be due to decreases in grain density or the formation of neutral complexes. For 5.700m/o, conductivity is lower than that pure of pure system [58-60].

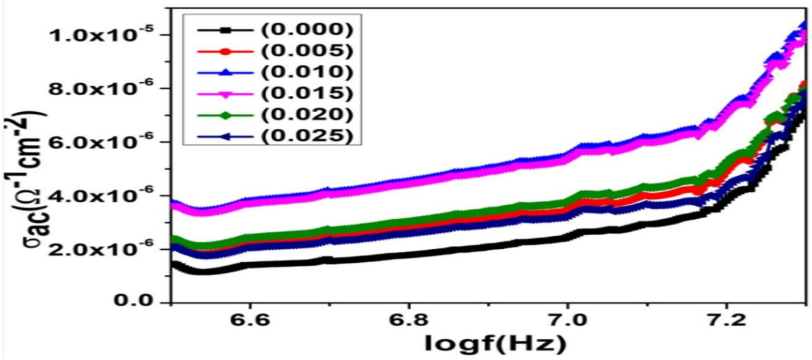


**Fig.9**. AC conductivity spectrum of $Co_{0.2}Mg_{0.8}Sm_xFe_{2-X}O_4$ nano-ferrites ( x= 0.000, 0.005, 0.010, 0.015, 0.020, and 0.025).

### 7.4. Real Impedance and Imaginary Impedance

Frequency dependent real and imaginary impedance spectra of frequency from 3Hz to 20MHz is shown in Figure 10 and 10 (b). See also real (Z') and imaginary impedance (Z").

$$Z' = |Z| \cos\theta z \quad (10)$$

$$Z'' = |Z| \sin\theta z \quad (11)$$

In all compositions, inter-facial polarization causes resistive grain barriers, resulting in high resistance. Less real and imaginary impedances mean more blending of impedance curves at higher frequencies [61, 64].

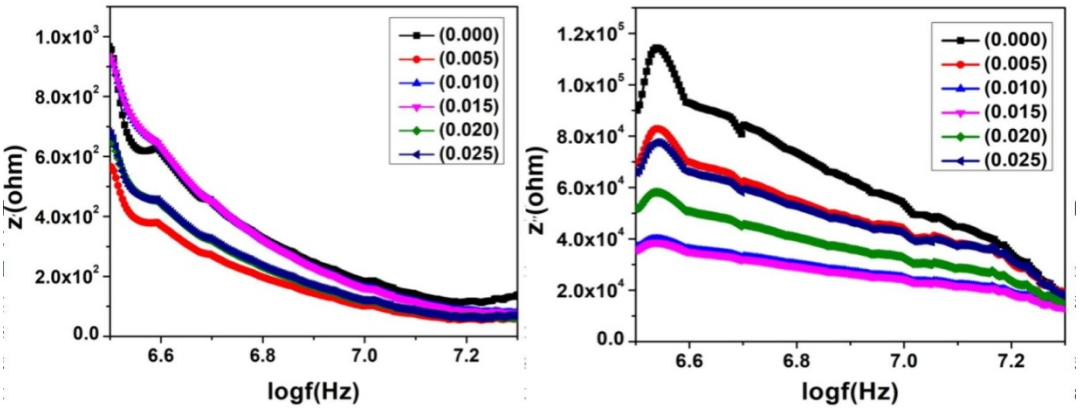


**Fig.10**.Variation of real part and imaginary part of impedance with frequency spectrum of $Co_{0.2}Mg_{0.8}Sm_xFe_{2-x}O_4$ nano-ferrites ( x= 0.000, 0.005, 0.010, 0.015, 0.020, and 0.025).

Impedance spectroscopy analysis was carried out to study the electrical and dielectracal properties of the material in the frequencies between 3Hz and 20MHz. The can also be used to separate of the contributions of electrical properties due to the grains, gain boundaries and electrode/ electrolyte interface in a polycrystalline material. Fig shows the impedance spectra of CMSFO system with varying m/o at 700°c. Frequency depend real and imaginary impedance response shown in Fig . For real impedance graph shows that at low frequency ranges the impedance is maximum, there after it appears to merge in the high frequency region which could be due to the relaxation of space charge, dipolar polarizations. For real impedance the sm doped Co-Mg-Fe is maximum for $9.0x10^4$, x= 0.000, Imaginary impedance is also similar to real and is the value is maximum for $9.5x10^2$, x = 0.015[65].

## 8. VIBRATING SAMPLE MAGNETOMETER (VSM)

Figure 11 shows nanosized $Co_{0.2}Mg_{0.8}Sm_xFe_{2-x}O4$ M-H loops ($x$ = 0, $0.00 \leq \chi \leq 0.025$). In M-H loops at ambient temperature, saturation magnetization (Ms), coercivity (Hc), retentivity (Mr), magnetic moment (B), squareness ratio (SQR), and anisotropy constant (K) have all been calculated. The obtained values are presented in Table 3 for the range of –18 to 18 Oe. The resulting saturation (Ms) in the range between 96.58-46.40 emu/g, Mr, Hc, and SQR, values are lowered, whereas Hc rises as the amount of $Sm^{+3}$ in the mixture increases. The loops for the produced samples evaluated at room temperature are relatively near to one another, suggesting extremely strong coercivity and typical super paramagnetic activity, as shown in Figure 11. The decrease in Ms with increase in particle size might be explained by cation

redistribution (exchange and substitution of cations in octahedral and tetrahedral sites) [66, 70]. The structure of $Co_{0.2}Mg_{0.8}Sm_xFe_{2-x}O_4$ transforms from an inverse spinel to a mixture spinel as the cations disperse. Ms decreases when x=0.005 until the nanoferrite with after which Ms slightly rises for the nanoferrite with x=0.010, and then Ms decreases again when x=0.025 is employed. The existence of a magnetically dead layer on the surface of the material, as well as a degree of spin canting over the whole volume of the crystallite structure, might explain the observed decrease in Ms. The quick rise in Ms for the nanoferrite with x=0.010 is due to an increase in the size of its crystallites, while the rapid increase in Ms for the nanoferrite with x=0.010 is due to an increase in the size of its crystallites [71-73]. A-A, B-B, and A-B super-exchange interactions, as well as A-B super-exchange interactions, are seen in spinel ferrites. The cation distribution between A and B varies as $Sm^{3+}$ dopes the ferrite, as does the intensity of the A-B exchange contact. A- sites get less $Fe^{3+}$ than B- sites when $Sm^{3+}$ ions are introduced. $Sm^{3+}$ most likely enters the octahedral site because to its large radius and tight tetrahedral A-site gap. The reduction in $Fe^{3+}$ concentration reduces the B-B exchange contact at the octahedral site, generating canting spins at the nanopartics surface. According to table 3, the saturation magnetization decreases when the net magnetic moment $B=M_B-M_A$ decreases ($M_A$ and $M_B$ are the Band A sublattice magnetic moments). When the concentration of $Sm^{3+}$ in CMSFO compositions is increased, the crystal lattice anisotropy decreases, resulting in a reduction in Mr [74]. Anisotropy increases until x= 0.0010, after which it decreases constantly until x= 0.025. The value of Hc increases as the concentration of $Sm^{3+}$ increases. This is owing to the permutation of $Co^{2+}$ ions with high magneto-crystalline anisotropy but low $Sm^{3+}$ion concentration. In fact, in addition to having non-quenched orbital angular momentum, $Co^{2+}$ion also possess a spin-orbit coupling. When spin-orbit coupling grows, magneto crystalline anisotropy rises, and materials containing cobalt ions become more coercive [75]. The corecivity of the nanoferrite with x=0.010 develops rapidly due to its high Ms Value. To overcome this spin alignment, a high value of Hc must be used. Because of the varied concentrations of $Sm^{3+}$, the squareness ratio decreases suddenly; it decreases for x = 0.005, increases for X = 0.010, and then decreases again for X = 0.025 [76.77].

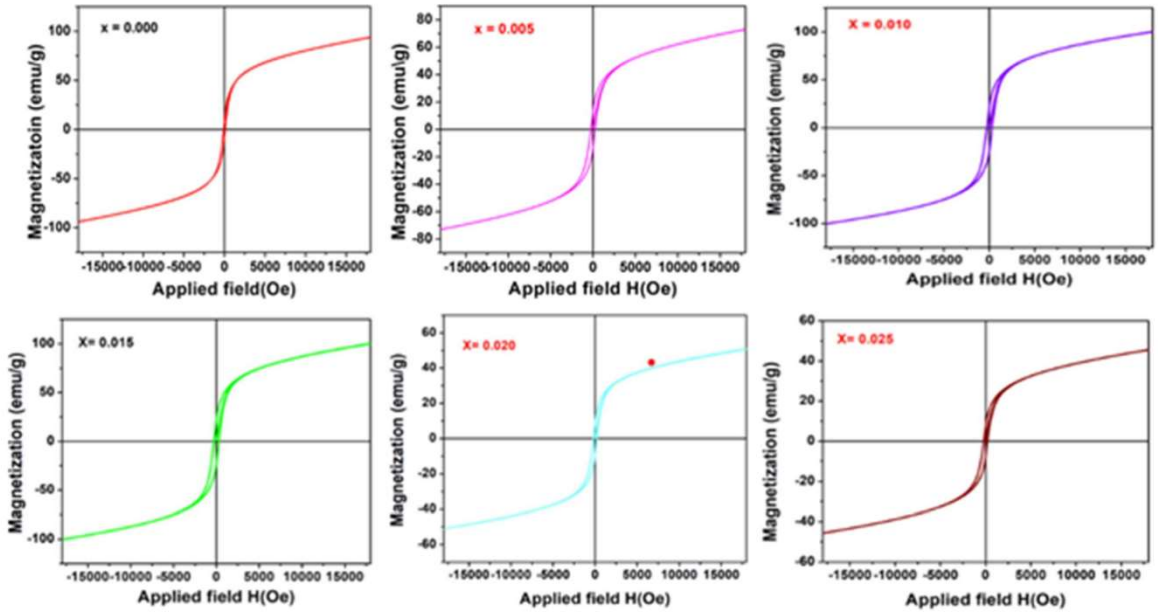


**Fig11**. M-H curves of nanosized $Co_{0.2}Mg_{0.8}Sm_xFe_{2-X}O_4$ nano-ferrites ( x= 0.000, 0.005, 0.010, 0.015, 0.020, and 0.025).

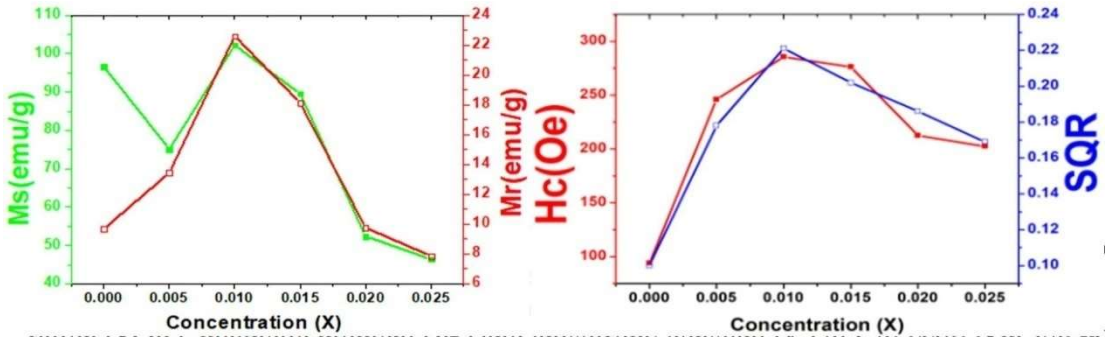


**Fig.12**. Saturation magnetization (Ms), retentively (Mr), and squareness ration Hc [Oe], coercively (SQR) spectrum of $Co_{0.2}Mg_{0.8}Sm_xFe_{2-x}O_4$ nano-ferrites ( x= 0.000, 0.005, 0.010, 0.015, 0.020, and 0.025).

Table3. The saturation magnetization (Ms), retentively (Mr), coercivity (Hc), squareness ration (SQR), magnetic moment ($\eta_B$) and anisotropy constant (K) of $Co_{0.2}Mg_{0.8}Sm_xFe_{2-X}O_4$; (Where $0.000 \leq x \leq 0.025$, step 0.005) nanoferrites.

| Sample code | $M_S$(emu/g) | $M_r$(emu/g) | Hc(Oe) | SQR | $\eta_B(\mu_B)$ | K(erg/cm$^3$) |
|---|---|---|---|---|---|---|
| 0.000 | 96.58 | 9.67 | 94.12 | 0.100 | 4.146 | 9275.622 |
| 0.005 | 75.11 | 13.44 | 246.08 | 0.178 | 3.321 | 18860.274 |
| 0.010 | 102.24 | 22.61 | 285.57 | 0.221 | 4.406 | 29792.527 |
| 0.015 | 89.54 | 18.14 | 276.26 | 0.202 | 3.866 | 25241.143 |
| 0.020 | 52.41 | 9.77 | 212.52 | 0.186 | 2.267 | 11365.482 |
| 0.025 | 46.40 | 7.86 | 202.46 | 0.169 | 2.011 | 9585.861 |

## 9. CONCLUSION

In this study, the citric sol gel auto combustion process is used to make samarium (Sm) substituted cobalt zinc ferrite (CoMgFe2O4) (range) nanoparticles. Because it is a straight forward and direct procedure. It can also be done in a natural setting. The mixing of solutions, stirring, drying, grinding, and annealing are the essential phases in this process. At 700°C, all of the prepared samples were sintered. Many studies have looked at the cations distribution of Sm- substituted ($CoMgFe_2O_4$) ferrite, and it has been found to be temperature dependent. The samples were found to be nicely crystalline spinel ferrite, which was regarded as a single phase ferrite, according to the XRD calculations. The crystallite size ranged from 21.32 to 26.74 nm, and the average lattice parameter was 8.03-8.89 (according to the XRD parameters). This is a highly useful approach for estimating crystalline characteristics, including strain, hopping length ($L_A$-$L_B$) site, dislocation density, bulk density, and X-ray density porosity. The XRDs most intense peak was reported at 2□=35°. The peak's locations and miller indices indicate the formation of an FCC spinel structure. According to the FESEM results, the particles are evenly dispersed, homogenous, and somewhat agglomerated. A TEM investigation revealed perfectly spherical and homogeneous nanocrystalline particles. TEM studies confirmed the nanoparticle sizes (74-80nm). A powerful ring of light surrounds the spinel ferrite sample in the SAED pattern. FTIR studies indicated two substantial peaks spanning from 395 cm-1 to 560 $cm^{-1}$, showing metal-oxygen stretching and the formation of ferrite composites. The material has Maxwell- Wagner interfacial polarization, which decreases as the frequency of the applied field rises, according to dielectric spectroscopy. With a dielectric loss of less than 8, the sample might be utilised to make multilayer inductors. The g-value was decreased and the spin-spin relaxation and the resonance magnetic field were increased by increasing the concentration of $Sm^{3+}$. The samples' Ac conductivity rose as doping and frequency were increased. The frequency window related to complex impedance appeared for x = 0.015 and x = 0.000 at room temperature in the frequency. At ambient temperature, saturation magnetization, coercively, and remanent magnetization from M-H loops were lowered when $Sm^{3+}$ was doped in zinc cobalt ferrite. The M-H loop analyses show the super paramagnetic behaviour of the prepared samples.

## ACKNOWLEDGMENT

Most of this study was done in the Materials Lab of Osmania University's Physics Department, with assistance from the University of Hyderabad's Physics Department (UOH)

## “DECLARATION OF COMPETING INTERESTS”

The authors declare that they have no known competing financial interests or personal relationships that could have appeared to influence the work reported in this paper.

## “RESEARCH DATE POLICY AND DATA AVAILABILITY STATEMENT”

Data available at the corresponding author will be provided on the request.

## REFERENCE.

1. F. Majid, S. Dildar, S. Ata, I. Bibi, I. Mohsin, A. Ali, M. Almoneef, M. Iqbal, S. Irshad, A. Nazir, M. Ali, Cobalt doping of nickel ferrites via sol gel approach: effect of doping

on the structural and dielectric properties, Z. fur Phys. Chem. 235 (12) (2021) 1811–1829, https://doi.org/10.1515/zpch-2021-3006.

2. M.D. Ali, T. Zeeshan, W. Tahir, Impact of Silver Substitution on Structural, Magnetic, Optical and Antibacterial Properties of Cobalt Ferrite, SSRN (2022) 32, https://doi.org/10.2139/ssrn.4167650.
3. Mohd. Hashim, Ateeq Ahmed, Syyed Asad Ali, Sagar E Shirsath, Mukhlis M Ismail, Ravi Kumar, Shalendra Kumar, Sher Singh Meena, D. Ravinder, Structural, optical, elastic and magnetic properties of Ce and Dy doped cobalt ferrites, J. Alloys Compd. 834 (2020) 5. 10.1016/j.jallcom.2020.155089.
4. Tetiana Tatarchuk, Maria Liaskovska, Volodymyr Kotsyubynsky, Mohamed Bououdina, Green synthesis of cobalt ferrite nanoparticles using Cydonia oblonga extract: structural and mossbauer studies, Mol. Cryst. Liq. Cryst. 13 (2019) 54-66 10.1080/15421406.2018.1542107.
5. S. Gubbala, H. Nathani, K. Koziol, R.D.K. Misra, Magnetic properties of nanocrystalline Ni–Zn, Zn–2, Mn, and Ni–Mn ferrites synthesized by reverse micelle technique, Phys. Rev. B Condens. Matter. 348 (2004) 317–328, https://doi. org/10.1016/j.physb.2003.12.017.
6. T. Zeeshan, S. Anjum, S. Waseem, F. Majid, M.D. Ali, A. Aslam, Influence of zinc substitution on structural, elastic, magnetic and optical properties of cobalt chromium ferrites, Mater. Sci.-Pol. 39 (1) (2021) 139–151, https://doi.org/ 10.2478/msp-2021-0008.
7. R. Verma, S. N. Kane, P. Tiwari, S.S. Modak, T. Tatarchuk, F. Mazaleyrat, Ni addition induced modification of structural, magnetic properties and antistructural modeling of Zn1-xNixFe2O4 (x = 0.0 - 1.0) nanoferrites, Mol. Cryst. Liq. Cryst. 674 (2019) 130-141 10.1080/15421406.2019.1578519.
8. E. Pervaiz, I. Gul, Enhancement of electrical properties due to Cr3+ substitution in Co-ferrite nanoparticles synthesized by two chemical techniques, J. Magn. Magn. Mater. 324 (2012) 3695–3703, https://doi.org/10.1016/j.jmmm.2012.05.050.
9. T. Tatarchuk, B. Al-Najar, M. Bououdina, M.A,A, Ahmed, Catalytic and Photocatalytic Properties of Oxide Spinels. In: Martínez, L., Kharissova, O., Kharisov, B. (Eds.) Handbook of Ecomaterials. Springer, Cham. 297 (2019) 1701–1750.
10. M. Sajjiaa, M. Oubahab, M. Hasanuzzamana, A.G. Olabic, Developments of cobalt ferrite nanoparticles prepared by the sol–gel process, Ceram. Int. 40 (2014) 1147. doi:10.1016/ j. ceramint.2013.06.116.
11. F. Majid, M.D. Ali, S. Ata, I. Bibi, A. Malik, A. Ali, M. Iqbal, Fe3O4/graphene oxide/ Fe4 [Fe (CN) 6] 3 nanocomposite for high performance electromagnetic interference shielding, Ceram. Int. 47 (8) (2021) 11587–11595.
12. M.D. Ali, F. Majid, A. Aslam, A. Malik, I. Wahid, S. Dildar, A.J.C.I. Dahshan, Dielectric and electrical properties of synthesized PBGO/Fe3O4 nanocomposite, Ceram. Int. 47 (18) (2021) 26224–26232, https://doi.org/10.1016/j. ceramint.2021.06.030.
13. G. Dascalu, T. Popescu, M. Federand, O.F. Caltun, Structural, electric and magnetic properties of CoFe1.8RE0.2O4 (RE = Dy, Gd, La) bulk materials, J. Magn. Magn. Mater. 333 (2013) 69-74. 10.1016/j.jmmm.2012.12.048.

14. C. Murugesan, G. Chandrasekaran, Impact of Gd3+ substitution on the structural, magnetic and electrical properties of cobalt ferrite nanoparticles, RSC Adv. 5 (2015) 73714–73725, https://doi.org/10.1039/C5RA14351A.
15. S. Waseem, T. Zeeshan, H. Tariq, F. Majid, M.D. Ali, Z.N. Kayani, M. Amami, The influence of transition metals (Fe, Co) on the structural, magnetic and optical properties of TiO2 nanoparticles synthesized by the hydrothermal method, Appl. Phys. A. 128 (8) (2022) 1–9, https://doi.org/10.1007/s00339-022-05749-w.
16. M.D. Ali, A. Aslam, T. Zeeshan, R. Mubaraka, S.A. Bukhari, M. Shoaib, S. Waseem, Robust effectiveness behavior of synthesized cobalt doped Prussian blue graphene oxide ferrite against EMI shielding, Inorg Chem Commun. 137 (2022), 109204, https://doi.org/10.1016/j.inoche.2022.109204.
17. K.D. Martinson, V.E. Belyak, D.D. Sakhno, A.A. Ivanov, L.A. Lebedev, L. A. Nefedova, I.B. Panteleev, V.I. Popkov, Solution combustion assisted synthesis of ultra-magnetically soft LiZnTiMn ferrite ceramics, J. Alloys Compd. 894 (2022), 162554, https://doi.org/10.1016/j.jallcom.2021.162554.
18. Y. Cedeno-Mattei, O. Perales-P´erez, O.N.C. Uwakweh, Y. Xin, Colossal roomtemperature coercivity in size-selected cobalt ferrite nanocrystals, J Appl. Phys. 107 (2010) 09A741, https://doi.org/10.1063/1.3339781.
19. K. Khaja Mohaideen, P.A. Joy, High magnetostriction and coupling coefficient for sintered cobalt ferrite derived from superparamagnetic nanoparticles, Appl. Phys. Let. 101 (2012), 072405, https://doi.org/10.1063/1.4745922.
20. M. El-Sayed Ahmed, M.A. Hamzawy Esmat, Structure and magnetic properties of NickeleZinc ferrite nanoparticles prepared by glass crystallization method, Monatsh fur Chemie/Chemical Mon. 137 (2006) 1119, https://doi.org/10.1007/ s00706-006-0521-1.
21. R. Jain, V. Luthra, M. Arora, Infrared Spectroscopic Study of Magnetic Behavior of Dysprosium Doped Magnetite Nanoparticles, J. Supercond. Nov. Magn. 32 (2019) 325–333, https://doi.org/10.1007/s10948-018-4717-5.
22. M.K. Shobana, H.S. Nam, H. Choe, The effects of lithium and yttrium substitution on the optical and structural properties of cobalt ferrites, Indian J. Phys. 93 (2019) 307–313, https://doi.org/10.1007/s12648-018-1292-3.
23. T. Tatarchuk, M. Bououdina, B. Al-Najar, R.B. Bitra, (2019). Green and Ecofriendly Materials for the Remediation of Inorganic and Organic Pollutants in Water. In: Naushad, M. (eds) A New Generation Material Graphene: Applications in Water Technology. Springer, Cham. 18 (2018) 69–110 10.1007/978-3-319-75484-0_4.
24. J.A. Moyer, C.A.F. Vaz, D.P. Kumah, D.A. Arena, V.E. Henrich, Enhanced magnetic moment in ultrathin Fe-doped CoFe2O4 films, Phys. Rev. B 17–1 (2012), 174404, https://doi.org/10.1103/PhysRevB.86.174404.
25. D. Gutierrez, M. Foerster, I. Fina, J. Fontcuberta, Dielectric response of epitaxially strained CoFe2O4 spinel thin films, Phys. Rev. B 86 (2012), 125309, https://doi. org/10.1103/PhysRevB.86.125309.
26. S. Soliman, A. Elfalaky, G.H. Fecher, C. Felser, Electronic structure calculations for ZnFe2O4, Phys. Rev. B. 83 (8–15) (2011), 085205, https://doi.org/10.1103/ PhysRevB.83.085205.

27. N. Ponpandian, A. Narayanasamy, N. Ponpandian, Grain size effect on the dielectric behavior of nanostructured Ni0.5Zn0.5Fe2O4, J Appl. Phys. A 101 (2007), 084116, https://doi.org/10.1063/1.2721379.
28. HyunhoShin VivekDhand, S.B. GyeonghunHan, SanghoonKim KyongyopRhee, Synthesis, characterization, and mechanical properties of oxygen-deficient ferrodiamagnetic transitional barium iron oxide perovskite/polydimethylsiloxane composites, J. Alloys Compd. 910 (2022), 164765, https://doi.org/10.1016/j. jallcom.2022.164765.
29. M. El-Sayed Ahmed, M.A. Hamzawy Esmat, Structure and magnetic properties of Nickel Zinc ferrite nanoparticles prepared by glass crystallization method, Monatsh fur Chemie/Chemical Mon. 137 (2006) 1119, https://doi.org/10.1007/s00706- 006-0521-1.
30. F. RavanelloMariosi, JanioVenturini, Alexandreda Cas Viegas, Carlos PerezBergmann, Lanthanum-doped spinel cobalt ferrite (CoFe2O4) nanoparticles for environmental applications, Ceram. Int. 46 (3) (2020) 2772–2779, https://doi. org/10.1016/j.ceramint.2019.09.266.
31. O. Michael, O.M. Strydom, Physical and magnetic properties of frustrated triangular-lattice antiferromagnets R3Cu (R = Ce, Pr), J. Alloys Compd. 895 (2022), 162545, https://doi.org/10.1016/j.jallcom.2021.162545.
32. Kiran Naz, Junaid Kareem Khan, Muhammad Khalid, Muhammad Saeed Akhtar, Zaheer Abbas Gilani, H M Noor u l Huda Khan Asghar, Gaber A. M. Mersal, Mohamed M. Ibrahim, Muhammad A, Ashiq M G B, 2022. Structural, dielectric, impedance and electric modulus analysis of Ni substituted copper spinel ferrites nanoparticles for microwave device applications. Mater Chem Phys. 285, 126091. DOI: 10.1016/j.matchemphys.2022.126091.
33. P.R. Mandal, S. Sahu, T.K. Nath, Microstructural, magnetic, and electrical properties of co–zn ferrites nanoparticles prepared by sol–gel method, Int. J. Nanosci. 1 (2011) 295–299, https://doi.org/10.1142/s0219581x11007946.
34. ZhijunMa ChangyeMang, MingjunRao JunLuo, ZhiweiPeng XinZhang, Electromagnetic wave absorption properties of cobalt-zinc ferrite nanoparticles doped with rare earth elements, J. Appl. Phys. 39 (2021) 1415–1426, https://doi. org/10.1016/j.jre.2020.08.011.
35. R.C. Kambale, K.M. Song, Y.S. Koo, N. Hur, Low temperature synthesis of nanocrystalline Dy doped cobalt ferrite: Structural and magnetic properties, J. Appl. Phys. 110 (2011), 053910, https://doi.org/10.1063/1.3632987.
36. S. Prathapani, M. Vinita, T.V. Jayaraman, D. Das, Structural and ambient/subambient temperature magnetic properties of Er-substituted cobalt-ferrites synthesized by sol-gel assisted auto-combustion method, J. Appl. Phys. 116 (2014), 023908, https://doi.org/10.1063/1.4889929.
37. F. Majid, I. Wahid, S. Ata, I. Bibi, M.D. Ali, A. Malik, A. Nazir, Cationic distribution of nickel doped NixCoX-1Fe2O4 nanparticles prepared by hydrothermal approach: Effect of doping on dielectric properties, Mater. Chem. Phys. 264 (2021), 124451, https://doi.org/10.1016/j.matchemphys.2021.124451.
38. Ravinder D, Hashim M, Upadhyay A, Ismail MM, Kumar S, Kumar R, et al. Investigation of structural and magnetic properties of La doped Co-Mn ferrite

nanoparticles in the presence of α-Fe2O3 phase. Solid State Commun. 2022, 342: 114629.

39. Shunmuga Priya R, Chaudhary P, Ranjith Kumar E, Balamurugan A, Srinivas C, Prasad G, et al. Effect of heat treatment on structural, morphological, dielectric and magnetic properties of Mg-Zn ferrite nanoparticles. Ceram. Int. 2022, 48(11): 15243.
40. Mahajan H, Godara SK, Srivastava AK. Synthesis and investigation of structural, morphological, and magnetic properties of the manganese doped cobalt-zinc spinel ferrite. J. Alloys Compd. 2022, 896: 162966.
41. Sertkol M, Güner S, Almessiere MA, Slimani Y, Baykal A, Gungunes H, et al. Effect of Bi3+ ions substitution on the structure, morphology, and magnetic properties of Co-Ni spinel ferrite nanofibers. Mater. Chem. Phys. 2022, 284: 126071.
42. Yadav RS, Havlica J, Masilko J, Kalina L, Hajdúchová M, Enev V, et al. Structural, Cation Distribution, and Magnetic Properties of CoFe2O4 Spinel Ferrite Nanoparticles Synthesized Using a Starch-Assisted Sol-Gel Auto-Combustion Method. J. Supercond. Nov. Magn. 2015, 28(6): 1851.
43. Lamouri R, Mounkachi O, Salmani E, Hamedoun M, Benyoussef A, Ez-Zahraouy H. Size effect on the magnetic properties of CoFe2O4 nanoparticles: A Monte Carlo study. Ceram. Int. 2020, 46(6): 8092.
44. Zi Z, Sun Y, Zhu X, Yang Z, Dai J, Song W. Synthesis and magnetic properties of CoFe2O4 ferrite nanoparticles. J. Supercond. Nov. Magn. 2009, 321(9): 1251.
45. Lamouri R, Fkhar L, Salmani E, Mounkachi O, Hamedoun M, Ait Ali M, et al. A combined experimental and theoretical study of the magnetic properties of bulk CoFe2O4. Appl. Phys. 2020, 126(5): 325.
46. Sharifianjazi F, Moradi M, Parvin N, Nemati A, Jafari Rad A, Sheysi N, et al. Magnetic CoFe2O4 nanoparticles doped with metal ions: A review. Ceram. Int. 2020, 46(11): 18391.
47. Kanithan S, Arun Vignesh N, Katubi KM, Subudhi PS, Yanmaz E, Arockia Dhanraj J, et al. Enhanced optical, magnetic, and photocatalytic activity of Mg2+ substituted NiFe2O4 spinel nanoparticles. J. Mol. Struct. 2022, 1265: 133289.
48. Patil DR, Chougule BK. Effect of copper substitution on electrical and magnetic properties of NiFe2O4 ferrite. Mater. Chem. Phys. 2009, 117(1): 35.
49. Ferreira LS, Silva TR, Silva VD, Raimundo RA, Simões TA, Loureiro FJA, et al. Spinel ferrite MFe2O4 (M = Ni, Co, or Cu) nanoparticles prepared by a proteic sol-gel route for oxygen evolution reaction. Adv. Powder Technol. 2022, 33(1): 103391.
50. Xie X, Wang B, Wang Y, Ni C, Sun X, Du W. Spinel structured MFe2O4 (M= Fe, Co, Ni, Mn, Zn) and their composites for microwave absorption: A review. Chem. Eng. J. 2022, 428: 131160.
51. Rose Vergis B, Kottam N, Hari Krishna R, Anil Kumar GN. Comparison of magnetic and dielectric properties of transition metal nanospinel ferrites, MFe2O4, (M = Co, Cu, Ni, Zn) synthesized by one-pot combustion route. Mater Today: Proceedings. 2022, 49: 870.
52. Yousaf M, Nazir S, Akbar M, Akhtar MN, Noor A, Hu E, et al. Structural, magnetic, and electrical evaluations of rare earth Gd3+ doped in mixed Co-Mn spinel ferrite nanoparticles. Ceram. Int. 2022, 48(1): 578. Journal Pre-proof

53. Almessiere, A.D. Korkmaz, Y. Slimani, M. Nawaz, S. Ali, A. Baykal, Magnetooptical properties of rare earth metals substituted Co-Zn spinel nanoferrites, Ceram. Int. 45 (2019) 3449–3458.
54. P.A. Vinosha, A. Manikandan, R. Ragu, A. Dinesh, K. Thanrasu, Y. Slimani, A. Baykal, B. Xavier, Impact of nickel substitution on structure, magneto-optical, electrical and acoustical properties of cobalt ferrite nanoparticles, J. Alloys Compd. 857 (2021) 157517.
55. M.T. Farid, I. Ahmad, M. Kanwal, G. Murtaza, M. Hussain, S.A. Khan, I. Ali, Synthesis, electrical and magnetic properties of Pr-substituted Mn ferrites for highfrequency applications, J. Electron. Mater. 46 (2017) 1826–1835.
56. J. Ghodake, R.C. Kambale, T. Shinde, P. Maskar, S. Suryavanshi, Magnetic and microwave absorbing properties of Co2+ substituted nickel–zinc ferrites with the emphasis on initial permeability studies, J. Magn. Magn Mater. 401 (2016) 938–942.
57. M. Yousaf, N. Mushtaq, B. Zhu, B. Wang, M.N. Akhtar, A. Noor, M. Afzal, Electrochemical properties of Ni0.4Zn0.6Fe2O4 and the heterostructure composites (Ni–Zn ferrite-SDC) for low temperature solid oxide fuel cell (LT-SOFC), Electrochim. Acta 331 (2020) 135349.
58. M.N. Islam, M. Harun-Or-Rashid, J. Islam, R. Parvin, A.A. Hossain, Improvement of microstructure and initial permeability of Mn0.5Ni0.1Zn0.4GdxFe2-xO4 with sintering temperature, Results in Physics 24 (2021) 104157.
59. K. Rady, M. Shams, Study the effect of Gd3+ incorporation into nanocrystalline (Ni–Ti) substituted Mn–Zn ferrites on its structure and functional properties, J. Magn. Magn Mater. 426 (2017) 615–620.
60. D.S. Mathew, R.-S. Juang, An overview of the structure and magnetism of spinel ferrite nanoparticles and their synthesis in microemulsions, Chem. Eng. J. 129 (2007) 51–65.
61. Y. Slimani, B. Unal, M. Almessiere, A.D. Korkmaz, S.E. Shirsath, G. Yasin, A. Trukhanov, A. Baykal, Investigation of structural and physical properties of Eu3 + ions substituted Ni0.4Cu0.2Zn0.4Fe2O4 spinel ferrite nanoparticles prepared via sonochemical approach, Results in Physics 17 (2020) 103061.
62. R. Zhang, L. Sun, Z. Wang, W. Hao, E. Cao, Y. Zhang, Dielectric and magnetic properties of CoFe2O4 prepared by sol-gel auto-combustion method, Mater. Res. Bull. 98 (2018) 133–138.
63. M. Abdellatif, G. El-Komy, A. Azab, Magnetic characterization of rare earth doped spinel ferrite, J. Magn. Magn Mater. 442 (2017) 445–452
64. . M. Abdellatif, A. Azab, M. Salerno, Effect of rare earth doping on the vibrational spectra of spinel Mn-Cr ferrite, Mater. Res. Bull. 97 (2018) 260–264.
65. M. Almessiere, Y. Slimani, M. Sertkol, H. Gungunes, Y. Wudil, A.D. Korkmaz, A. Baykal, Impact of Gd substitution on the structure, hyperfine interactions, and magnetic properties of Sr hexaferrites, Ceram. Int. (2021).
66. R.R. Kanna, N. Lenin, K. Sakthipandi, A.S. Kumar, Structural, optical, dielectric and magnetic studies of gadolinium-added Mn-Cu nanoferrites, J. Magn. Magn Mater. 453 (2018) 78–90.

67. M. Shahid, S. Shafi, M.F.A. Aboud, M.F. Warsi, M. Asghar, I. Shakir, Impacts of Co2 + and Gd3+ co-doping on structural, dielectric and magnetic properties of MnFe2O4 nanoparticles synthesized via micro-emulsion route, Ceram. Int. 43 (2017) 14096–14100.
68. R.R. Kanna, N. Lenin, K. Sakthipandi, M. Sivabharathy, Impact of lanthanum on structural, optical, dielectric and magnetic properties of Mn1-xCuxFe1.85La0.15O4 spinel nanoferrites, Ceram. Int. 43 (2017) 15868–15879.
69. M.F. Warsi, A. Iftikhar, M.A. Yousuf, M.I. Sarwar, S. Yousaf, S. Haider, M.F. A. Aboud, I. Shakir, S. Zulfiqar, Erbium substituted nickel–cobalt spinel ferrite nanoparticles: tailoring the structural, magnetic and electrical parameters, Ceram. Int. 46 (2020) 24194–24203.
70. M.N. Akhtar, H.A. Siddiqa, M.S. Nazir, M.A. Khan, Preparations and tailoring of structural, magnetic properties of rare earths (REs) doped nanoferrites for microwave high frequency applications, Ceram. Int. 46 (2020) 26521–26529.
71. R.S. Yadav, J. Havlica, J. Masilko, L. Kalina, J. Wasserbauer, M. Hajdúchova, ´ V. Enev, I. Kuˇritka, Z. Koˇz´ akov´ a, Impact of Nd3+ in CoFe2O4 spinel ferrite nanoparticles on cation distribution, structural and magnetic properties, J. Magn. Magn Mater. 399 (2016) 109–117.
72. H.-M. Fan, J.-B. Yi, Y. Yang, K.-W. Kho, H.-R. Tan, Z.-X. Shen, J. Ding, X.-W. Sun, M.C. Olivo, Y.-P. Feng, Single-crystalline MFe2O4 nanotubes/nanorings synthesized by thermal transformation process for biological applications, ACS Nano 3 (2009) 2798–2808.
73. G. Dascalu, T. Popescu, M. Feder, O. Caltun, Structural, electric and magnetic properties of CoFe1.8RE0.2O4 (RE= Dy, Gd, La) bulk materials, J. Magn. Magn Mater. 333 (2013) 69–74.
74. A. Raut, R. Barkule, D. Shengule, K. Jadhav, Synthesis, structural investigation and magnetic properties of Zn2+ substituted cobalt ferrite nanoparticles prepared by the sol–gel auto-combustion technique, J. Magn. Magn Mater. 358 (2014) 87–92.
75. W. Zhang, A. Sun, X. Zhao, X. Pan, Y. Han, N. Suo, L. Yu, Z. Zuo, Structural and magnetic properties of Ni–Cu–Co ferrites prepared from sol-gel auto combustion method with different complexing agents, J. Alloys Compd. 816 (2020) 152501.
76. R.S. Yadav, I. Kuˇritka, J. Vilcakova, J. Havlica, L. Kalina, P. Urb´ anek, M. Machovsky, D. Skoda, M. Masaˇr, M. Holek, Sonochemical synthesis of Gd3+ doped CoFe2O4 spinel ferrite nanoparticles and its physical properties, Ultrason. Sonochem. 40 (2018) 773–783.
77. M. Almessiere, Y. Slimani, M. Sertkol, F. Khan, M. Nawaz, H. Tombuloglu, E. AlSuhaimi, A. Baykal, Ce–Nd Co-substituted nanospinel cobalt ferrites: an investigation of their structural, magnetic, optical, and apoptotic properties, Ceram. Int. 45 (2019) 16147–16156.